PROCEEDINGS of the
23rd International Congress on Acoustics

9 to 13 September 2019 in Aachen, Germany

Study on large scale projectile impact point positioning method based on trajectory shock wave

Difeng SUN[1]; Xubin LIANG[1]; Tianqing ZHAO[1]; Houlin FANG[1]; Zhang CHENG[1]; Hui ZHENG[1]; Liangyong ZHANG[1]; Fang ZHANG[1]; Deyu SUN[1]; Yang LIU[1]

[1] Northwest Institute of Nuclear Technology, China

ABSTRACT

With multiple nodes of single acoustic sensor layed around the target, the ballistic shock wave signal of the projectile generated before hitting the ground can be detected at different locations. The trajectory can be estimated by measuring the time difference between the signal of different nodes, and the impact point can be coordinated by crossing the trajectory with the target. In this article, the projectile impact point positioning model is parameterised and fomulated by nonlinear equations with six patameters, and it can be solved by means of nonlinear least square (NLS) method. By means of Cramer-Rao lower bound (CRLB) analysis, measurement error distribution by different incident angle and different impact location is calculated, and also, parameter of exterior ballistics model and wind vector is under consideration.
Keywords: Impact Point Positioning, Projectory Trajectory, CRLB

1. INTRODUCTION

When the projectile flies in the air at supersonic speed, its front end sharply compresses the air in front, forming shock wave(1, 2). As it diffuses, the shock wave gradually degenerates into weak compression wave, and the propagation speed drops from supersonic to sound, finally forming the cone wavefront(3).

At the sensor, the shock wave is measured in the form of N-wave(4). The trajectory of the projectile can be estimated according to the arrival time of the N-wave measured at different positions. The intersection point between the trajectory and the ground or obstacles is the projectile impact point(5). In early work, the ballastic equation of motion was studied(6). Ballistic const C_b was introduced to describe the air resistance effect(7). If the gravitational acceleration g is ignored, the ballistic trajectory will be linear. Researches show that with ballistic constant C_b known and drag coefficient exponent η=0.5, the trajectory parameter and impact point can be well estimated(7).

In this paper, the impact point is estimated in the case that sensor coordinates and sound speed are not exactly measured or presumed. Also, the influence of wind on sound speed vector is coarsely modeled. This paper focuses on the study on error analysis method based on Cramer-Rao lower bound (CRLB)(8). Through numerical simulation and CRLB method, the error distribution rule of impact point for large scale target is obtained, and then other scale targets are also taken into account.

2. PROBLEM MODELING

2.1 Basic assumptions

In order to simplify the model of supersonic flight projectile ballistic shock wave, some assumptions are made. 1) The near-field nonlinear region of projectile is ignored and the velocity of shock wave is considered as sound speed. 2) The curvilinear induced by gravity acceleration g is ignored since its acting time is too short. 3) After the projectile hits the ground, its motion equation changes and some sensors' signal data is affected. But here, this process is omitted since it can be solved in other ways such as excluding the abnormal sensors.

2.2 Geometric Model

Geometric model settings are similar to that in literature(9), as shown in Figure 1(a). N sensors S_n

[1] sundifeng@nint.ac.cn

are located in the target perimeter with position vector $\mathbf{R}_n=[X_n,Y_n,0]^{\mathrm{T}}$.The projectile hit the ground at a certain elevation angle θ and azimuth angle ϕ, on point Q with vector $\mathbf{R}_Q=[X_Q,Y_Q,0]^{\mathrm{T}}$. The unit direction vector of trajectory is $\mathbf{e}_v$=-[cosθcosϕ, cosθsinϕ, sinθ]$^{\mathrm{T}}$. In the plane $\boldsymbol{\pi}_n$ which determined by linear trajectory and sensor S_n, a triangle is formed by the hitting point Q, the sensor point S_n and the detach point $\mathrm{P_n}$. The parameter set $\boldsymbol{\lambda}=\{X_Q,Y_Q,\theta,\phi,V_r\}$, is what we focus on, especially impact point coordiantes X_Q and Y_Q in it.

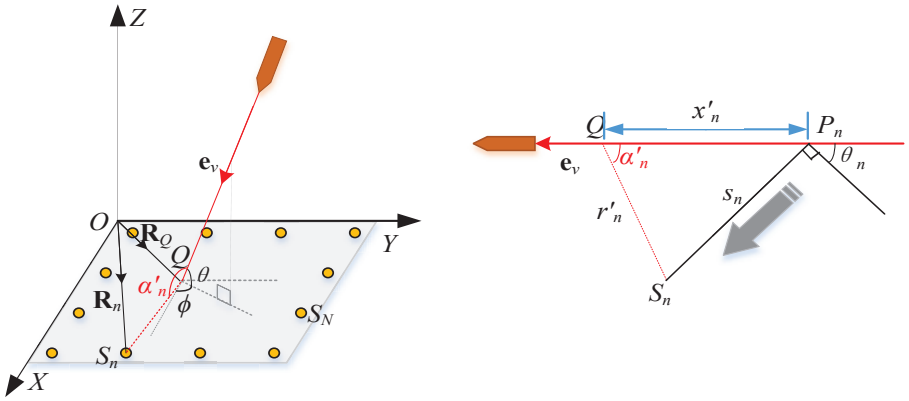

(a) (b)

Figure 1 – (a) Geometric distribution of the sensors. The linear trajectary intersects the ground at Q

(b)Ballistic shock wave reach sensor S_n

2.3 Mathematical model

In the ballistic model, g is ignored, the ballistic constant C_b is known and drag coefficient exponent η=0.5. The instantaneous velocity $v'(x')$ at x' and the flight time $t'(x')$ from a reference point to $\mathrm{P_n}$ are calculated as in literature(9).

The time stamp of shock wave arriving at S_n is given by Equation (1) and s_n is calculated with sine theory in triangle P_nQS_n.

$$\tau_n = t'(x'_n) + s_n / c \tag{1}$$

The Differencial Time of Arrival (DTOA)(9) between Sensors S_m and $S_n\,(1\le m,n\le N)$:

$$\tau_{nm} = \tau_n - \tau_m = t'(x'_n) - t'(x'_m) + (s_n - s_m)/c \tag{2}$$

2.4 NLS Method

The estimated value of DTOA can be expressed as:

$$\hat{\mathbf{b}}(\hat{\boldsymbol{\tau}}) = \mathbf{b}(\boldsymbol{\lambda};\hat{\mathbf{R}},\hat{c},\hat{C}_b) + \mathbf{n} \tag{3}$$

Where $\hat{\mathbf{b}}=[\hat{\tau}_{21},\hat{\tau}_{31},\ldots,\hat{\tau}_{N1}]^{\mathrm{T}}$, $\mathbf{b}=[\tau_{21},\tau_{31},\ldots,\tau_{N1}]^{\mathrm{T}}$ and $\mathbf{n}=[n_1,n_2,\ldots n_{N-1}]^{\mathrm{T}}$ are respectively the observation vector, the model value vector and the total observation error vector of DTOA. The caret "^" on a certain variable represents an observation, presumption or estimation of the actual value or presetting value. $\hat{\boldsymbol{\tau}}=[\hat{\tau}_1,\hat{\tau}_2,\ldots,\hat{\tau}_N]^{\mathrm{T}}$, $\hat{\mathbf{R}}=[\hat{X}_1,\hat{Y}_1,\hat{X}_2,\hat{Y}_2,\ldots\hat{X}_N,\hat{Y}_N]^{\mathrm{T}}$, $\hat{c}$, $\hat{C}_b$ are respectively the observation or the presumption value (vector) of arrival time stamp vector $\boldsymbol{\tau}=[\tau_1,\tau_2,\ldots,\tau_N]^{\mathrm{T}}$, sensor coordination vector $\mathbf{R}=[X_1,Y_1,X_2,Y_2,\ldots X_N,Y_N]^{\mathrm{T}}$, sound speed c and ballistic constant C_b, with observation or presumption error $\mathbf{n}_{\boldsymbol{\tau}}=[n_{\tau 1},n_{\tau 2},\ldots n_{\tau N}]$, $\mathbf{n}_{\mathbf{R}}=[n_{X1},n_{Y1},n_{X2},n_{Y2},\ldots n_{XN},n_{YN}]$, n_c, n_{C_b}. Besides, the observation error vector of DTOA caused by the sampling procedure can be described as $\mathbf{n}_{\mathbf{b}}=[n_{\tau 2}-n_{\tau 1},n_{\tau 2}-n_{\tau 1},\ldots n_{\tau \mathrm{N}}-n_{\tau 1}]^{\mathrm{T}}$. $\boldsymbol{\lambda}=\{X_Q,Y_Q,\theta,\phi,V_r\}$ is the set of unknown parameter to resolve. Use a (N-1) demensional column vector $\mathbf{F}$ to describe the total error between observation vector and model vector.

$$\mathbf{F}(\boldsymbol{\lambda};\hat{\boldsymbol{\tau}},\hat{\mathbf{R}},\hat{c},\hat{C}_b) = \hat{\mathbf{b}}(\hat{\boldsymbol{\tau}}) - \mathbf{b}(\boldsymbol{\lambda};\hat{\mathbf{R}},\hat{c},\hat{C}_b) \tag{4}$$

Non-linear Least Square (NLS) method(9) can be used to estimate $\boldsymbol{\lambda}$ with Equation (11):

$$\hat{\boldsymbol{\lambda}} = \arg\min_{\boldsymbol{\lambda}'} \mathbf{F}(\boldsymbol{\lambda}';\hat{\boldsymbol{\tau}},\hat{\mathbf{R}},\hat{c},\hat{C}_b)^{\mathrm{T}}\mathbf{N}^{-1}\mathbf{F}(\boldsymbol{\lambda}';\hat{\boldsymbol{\tau}},\hat{\mathbf{R}},\hat{c},\hat{C}_b) \tag{5}$$

Since the observation error covariance matrix of DTOA is usually unknown, an assumed error convariance matrix $\hat{\mathbf{N}} = \sigma^2(\mathbf{I}+\mathbf{E})$ is alternative. In this formula, σ^2 is the arrival time stamp error caused by the sampling procedure, $\mathbf{I}$ is the (N-1)×(N-1) identity matrix and $\mathbf{E}$ is the unit matrix. Equation (11) can be solved by numerical iterative algorithm.

3. ERROR ANALYSIS AND CRLB METHOD

3.1 Error Source Analysis

Traditional methods generally assume that the error of DTOA of two sensors is only caused by the signal acquisition process. But in reality, it's also indirectly influenced by various factors during the flight.

The position error of sensors will affect the total distance of shock wave propagation in the air(10).

The different choice of trajectory model has a great influence on the impact point positioning problem. The ballistic constant C_b is one of the parameters of the model. In this paper, C_b is supposed to be already known.

The shock wave speed is mainly affected by wind, if tempearture factor is ignored. The influence of the wind should be the key to consider when the test is done outside(11), while most articles choose to ignore its impact because it's too complex.

3.2 Coarse One Dimensional Wind Modeling

It's difficult to use a general method for wind modeling. Ignoring its influence on the trajectory of projectile, wind mainly affects the velocity and direction of shock wave propagation relative to the earth. The wind is momentarily uniform for small area, but has strong inhomogeneity, instantaneity and randomness for large area. As shown in Figure 2, the effect of wind speed of the same amplitude on sound vector is equivalent to adding a circle whose center point is at the end of sound vector and radius is equal to wind speed amplitude.

$$\mathbf{c}' = \mathbf{c} + \mathbf{w} \tag{6}$$

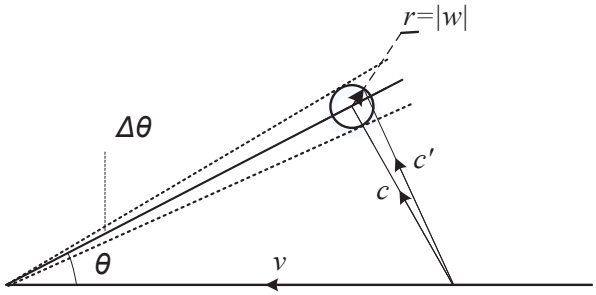

Figure 2 – Influence of wind on sound speed

The shock wave speed vector, namely the revised sound speed vector $\mathbf{c}'$ is influenced by wind speed vector $\mathbf{w}$. Since the amplitude of wind w is far less than sound speed c, the change of shock wave angle $\Delta\theta$ is also far less than original angle θ. The maximum and minimum influence of wind is obtained when revised angle $\theta' = \arcsin(c'/v)$ meets the extreme value. Since $w \ll c$, $\mathbf{c}'$ and $\mathbf{c}$ is approximately parallel and Equation (13) can be concluded.

$$c'_{\max} \approx c + w \qquad c'_{\min} \approx c - w \tag{7}$$

Between the maximum and minimun influence of wind, appropriate intersection of wind distribution can be used to simply construct the wind model, in this way wind can be modeled in the same (or opposite) direction of sound speed. A gaussion distribution of wind w is finally used in convenience.

In this paper, the error of c from temperature is omitted, then we see that $\hat{c} = c'$ and $n_c = w$, i.e. the distribution of sound speed error is the same as the distribution of wind w. Although this one-dimensional model leads to linear error distribution of impact point(as shown below in this

paper), which may not fit actual situation, the amplitude of error yet has reference value.

3.3 CRLB Error Analysis

Assume that the observation error vector $\mathbf{n}$ follows the zero-mean Gaussian distribution, with convariance matrix $\mathbf{N}$. When the observation (or presumption) of arrival time stamp $\hat{\boldsymbol{\tau}}$, sensor coordinate $\hat{\mathbf{R}}$, sound speed $\hat{c}$ and ballistic constant $\hat{C}_b$ is known, the CRLB on conviance matrix is as shown(12, 13):

$$\mathbf{Q}(\boldsymbol{\lambda};\hat{\boldsymbol{\tau}},\hat{\mathbf{R}},\hat{c},\hat{C}_b)=[\nabla\mathbf{F}^{\mathrm{T}}\mathbf{N}^{-1}(\nabla\mathbf{F}^{\mathrm{T}})^{\mathrm{T}}]^{-1} \tag{8}$$

Where $\nabla=[\partial/\partial X_Q,\partial/\partial Y_Q,\partial/\partial\theta,\partial/\partial\phi,\partial/\partial V_r]^{\mathrm{T}}$ is the gradient operator, and $\nabla\mathbf{F}^{\mathrm{T}}$ can be estimated by the observation or presumption value $\{\hat{\boldsymbol{\tau}},\hat{\mathbf{R}},\hat{c},\hat{C}_b\}$ and presetted value $\boldsymbol{\lambda}$.

The total observation error vector $\mathbf{n}$ is determined by many aspects. Ignoring second and higher order small terms, use first order Taylor expansion to describe the propagation law of error, we get:

$$\begin{aligned}\mathbf{F}(\boldsymbol{\lambda};\hat{\boldsymbol{\tau}},\hat{\mathbf{R}},\hat{c},\hat{C}_b)-\mathbf{F}(\boldsymbol{\lambda};\boldsymbol{\tau},\mathbf{R},c,C_b)&=\sum_{\theta\in\{\boldsymbol{\tau},\mathbf{R},c,C_b\}}\frac{\partial\mathbf{F}}{\partial\theta}\cdot(\hat{\theta}-\theta)\\&=\sum_{\tau\in\{\boldsymbol{\tau}\}}\frac{\partial\mathbf{F}}{\partial\tau}\cdot(\hat{\tau}-\tau)+\sum_{X\in\{\mathbf{R}\}}\frac{\partial\mathbf{F}}{\partial X}\cdot(\hat{X}-X)+\frac{\partial\mathbf{F}}{\partial c}(\hat{c}-c)+\frac{\partial\mathbf{F}}{\partial C_b}(\hat{C}_b-C_b)\\&=(\hat{\mathbf{b}}-\mathbf{b})+\sum_{X\in\{\mathbf{R}\}}\frac{\partial\mathbf{F}}{\partial X}\cdot(\hat{X}-X)+\frac{\partial\mathbf{F}}{\partial c}(\hat{c}-c)+\frac{\partial\mathbf{F}}{\partial C_b}(\hat{C}_b-C_b)\end{aligned} \tag{9}$$

$$\mathbf{n}=\mathbf{n}_{\mathbf{b}}+\sum_{X\in\{\mathbf{R}\}}\frac{\partial\mathbf{F}}{\partial X}\cdot n_X+\frac{\partial\mathbf{F}}{\partial c}\cdot n_c+\frac{\partial\mathbf{F}}{\partial C_b}\cdot n_{C_b} \tag{10}$$

$\{\boldsymbol{\tau},\mathbf{R},c,C_b\}$ is the set of all elements in $\boldsymbol{\tau},\mathbf{R},c,C_b$, $\{\boldsymbol{\tau}\}$, $\{\mathbf{R}\}$ have the similar meaning. The function value of $\mathbf{F}$ of different paramaters $\hat{\boldsymbol{\tau}},\hat{\mathbf{R}},\hat{c},\hat{C}_b$ and $\boldsymbol{\tau},\mathbf{R},c,C_b$ represents the total observation error calculated by parameters with certain error distribution or not. $\mathbf{F}(\hat{\theta})$ $\theta\in\{\boldsymbol{\tau},\mathbf{R},c,C_b\}$ represents the function value of all exact parameters except θ. $\mathbf{F}(\boldsymbol{\lambda};\boldsymbol{\tau},\mathbf{R},c,C_b)=\mathbf{0}$ from definition, and $\mathbf{F}$ is the abbreviation of $\mathbf{F}(\boldsymbol{\lambda};\boldsymbol{\tau},\mathbf{R},c,C_b)$. Suppose all $n\in\{\mathbf{n}_{\boldsymbol{\tau}},\mathbf{n}_{\mathbf{R}},n_c,n_{C_b}\}$ are independent identically distributed and follow zero-mean Gaussian distribution, we have:

$$\begin{aligned}\mathbf{N}_{\mathbf{b}}&=\mathrm{E}(\mathbf{n}_{\mathbf{b}}\cdot\mathbf{n}_{\mathbf{b}}^{\mathrm{T}})\\&=\mathrm{E}([n_{\boldsymbol{\tau},2}-n_{\boldsymbol{\tau},1},n_{\boldsymbol{\tau},2}-n_{\boldsymbol{\tau},1},\ldots n_{\boldsymbol{\tau},\mathrm{N}}-n_{\boldsymbol{\tau},1}]^{\mathrm{T}}\cdot[n_{\boldsymbol{\tau},2}-n_{\boldsymbol{\tau},1},n_{\boldsymbol{\tau},2}-n_{\boldsymbol{\tau},1},\ldots n_{\boldsymbol{\tau},\mathrm{N}}-n_{\boldsymbol{\tau},1}])\\&=\sigma_{\boldsymbol{\tau}}^2(\mathbf{I}+\mathbf{E})\end{aligned} \tag{11}$$

$$\begin{aligned}\mathbf{N}&=\mathrm{E}(\mathbf{n}\cdot\mathbf{n}^{\mathrm{T}})\\&=\mathbf{N}_{\mathbf{b}}+\mathrm{E}[\mathbf{F}(\sum_{X\in\{\mathbf{R}\}}\frac{\partial}{\partial X}\cdot n_X+\frac{\partial}{\partial c}\cdot n_c+\frac{\partial}{\partial C_b}\cdot n_{C_b})\cdot(\sum_{Y\in\{\mathbf{R}\}}\frac{\partial}{\partial Y}\cdot n_X+\frac{\partial}{\partial c}\cdot n_c+\frac{\partial}{\partial C_b}\cdot n_{C_b})\mathbf{F}^{\mathrm{T}}]\\&=\sigma_{\boldsymbol{\tau}}^2(\mathbf{I}+\mathbf{E})+\sigma_{\mathbf{R}}^2(\sum_{X\in\{\mathbf{R}\}}\frac{\partial\mathbf{F}}{\partial X}\frac{\partial\mathbf{F}^{\mathrm{T}}}{\partial X})+\sigma_c^2(\frac{\partial\mathbf{F}}{\partial c}\frac{\partial\mathbf{F}^{\mathrm{T}}}{\partial c})+\sigma_{C_b}^2(\frac{\partial\mathbf{F}}{\partial C_b}\frac{\partial\mathbf{F}^{\mathrm{T}}}{\partial C_b})\end{aligned} \tag{12}$$

$\mathbf{N}_{\mathbf{b}}$ is the DTOA error covariance matrix caused by sampling procedure, and $\mathbf{N}$ is the total DOTA observation error covariance matrix. $\sigma_{\boldsymbol{\tau}},\sigma_{\mathbf{R}},\sigma_c,\sigma_{C_b}$ are the corresponding standard deviation. From Equation (10) we can conclude that $\mathbf{N}$ follows indeed the zero-mean Gaussion distribution if all relevant error distributions follow zero-mean Gaussion distribution. $\mathbf{n}$ and $\mathbf{N}$ are both made up of four terms and influenced by them.

In special cases, if the last three term are zero or can be negelected, then

$$\mathbf{n}=\mathbf{n}_{\mathbf{b}}=\hat{\mathbf{b}}(\hat{\boldsymbol{\tau}})-\mathbf{b}(\boldsymbol{\lambda};\mathbf{R},c,C_b),\mathbf{N}=\mathbf{N}_{\mathbf{b}}=\sigma_{\boldsymbol{\tau}}^2(\mathbf{I}+\mathbf{E}) \tag{13}$$

This is in accordance with traditional methods(7, 9, 11).

4. SIMULATION RESULTS

4.1 Simulation Setting

Suppose the square target is on the ground plane with side length of $4a$ (a is the sensor spacing and represents the scale of target), and N=16 sound detection nodes of single sensor are uniformly distributed around it, as shown in Figure 1(a). The position vectors of N sensors are $\mathbf{R}_1$=[0,0,0], $\mathbf{R}_2$=[0,a,0], etc. The standand deviation of X, Y and Z-coordinates is 3cm. Suppose the ballistic constant C_b=150 is exactly known in advance. Considering winds within gentle breeze (0~5.4m/s), the standard derivation of shock wave speed, namely the standard derivation of wind is set to 2.7m/s. Suppose the arrival time stamp error caused by signal acqusition procedure is 10μs.

Computer simulations were carried out with MATLAB. To simulate a particular scenario, true value $\boldsymbol{\lambda}=\{X_Q,Y_Q,\theta,\phi,V_r\}$ with erroneous $\hat{\mathbf{R}},\hat{c}$ and presetted value C_b was used to generate DTOA observation value $\hat{\mathbf{b}}$ and then would be forgotten, see literature(9) for detailed calculation method. Then with $\hat{\mathbf{R}},\hat{c},C_b$ and $\hat{\mathbf{b}}$ known , $\hat{\boldsymbol{\lambda}}=\{\hat{X}_Q,\hat{Y}_Q,\hat{\theta},\hat{\phi},\hat{V}_r\}$ could be resolved by NLS method with reference to Equation (4) and (5). For each scenario, simulations were carried out for 100 times.

CRLB on the DTOA error covariance matrix was calculated for every scenario with Equation (8), in which error covariance matrix $\mathbf{N}$ refers to Equation (12).

4.2 Influence of Error Sources on Simulation Results

This is Scenario 1, set a=50. In this 200×200m target area, the projectile hits the ground at point Q(80,90,0)m with an elevation angle π/3 and azimuth angle 0, and the impact velocity is 700m/s. Then the positioning error of the projectile impact point is simulated in the following cases.

Scenario 1.1 Only DTOA error caused by signal acquisition process is taken into account, 100 times of simulations are carried out to calculate impact point position, its mean value and one standard derivation (1-SD) ellipse, then actual value and CRLB ellipse are shown to compare in Figure 3(a).

Scenario 1.2 Only DTOA error caused by sensor position error is taken into account, and simulation results are shown in Figure 3(b).

Scenario 1.3 Only DTOA error caused by wind, namely sound speed error is taken into account, and simulation results are shown in Figure 3(c).

Scenario 1.4 All DTOA error sources in Scenerio 1.1~1.3 are taken into account, and results are shown in Figure 3(d).

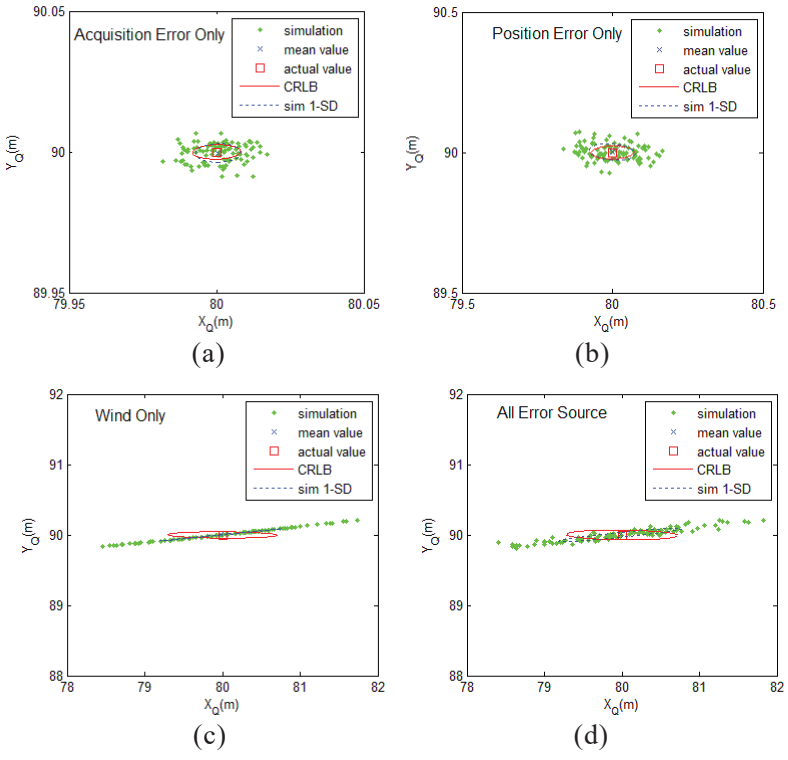

Figure 3 – Simulation results for different error source. (a)-(d) show the estimation results of Scenerio 1.1-1.4. Dots donate estimates from 100 times of simulation value, crosses donate mean values of simulation, squares denote the actual values, solid lines denote CRLB error ellipses, and dashed lines denote 1-SD error ellipses.

As can be seen from the above figure, error discription method of CRLB fits the simulation of projectile impact point well. To targets of large area, the influence of arrival time acquisition error is the smallest, the sensor coordinate error is the second, while the influence of wind speed is the greatest. The total error is mainly affected by the wind speed.

In this scenario, the elevation angle $\theta=\pi/3$ and the azimuth angle $\phi=0$, so the projection of trajectory parallels the X-axis, so the X-coordinate is mainly affected. The arrival time of Sensor 1 is subtracted in every equation of DTOA algorithm, resulting in the asymmetry of simulated impact point coordinate distribution.

4.3 Positioning Error Vary with Trajectory Parameters

This is Scenario 2, and the basic setting is the same as Scenario 1. All error sources are considered, and specific parameters vary in a certain range to obtain the distribution of CRLB stand deviation of DTOA.

Scenario 2.1 Scan X_Q and Y_Q, the CRLB standard deviation distribution of X_Q, Y_Q and R_Q is shown in Figure 4(a), (b) and (c).

Scenario 2.2 Scan θ and ϕ, the CRLB standard deviation distribution of X_Q, Y_Q and R_Q is shown in Figure 4(d), (e) and (f).

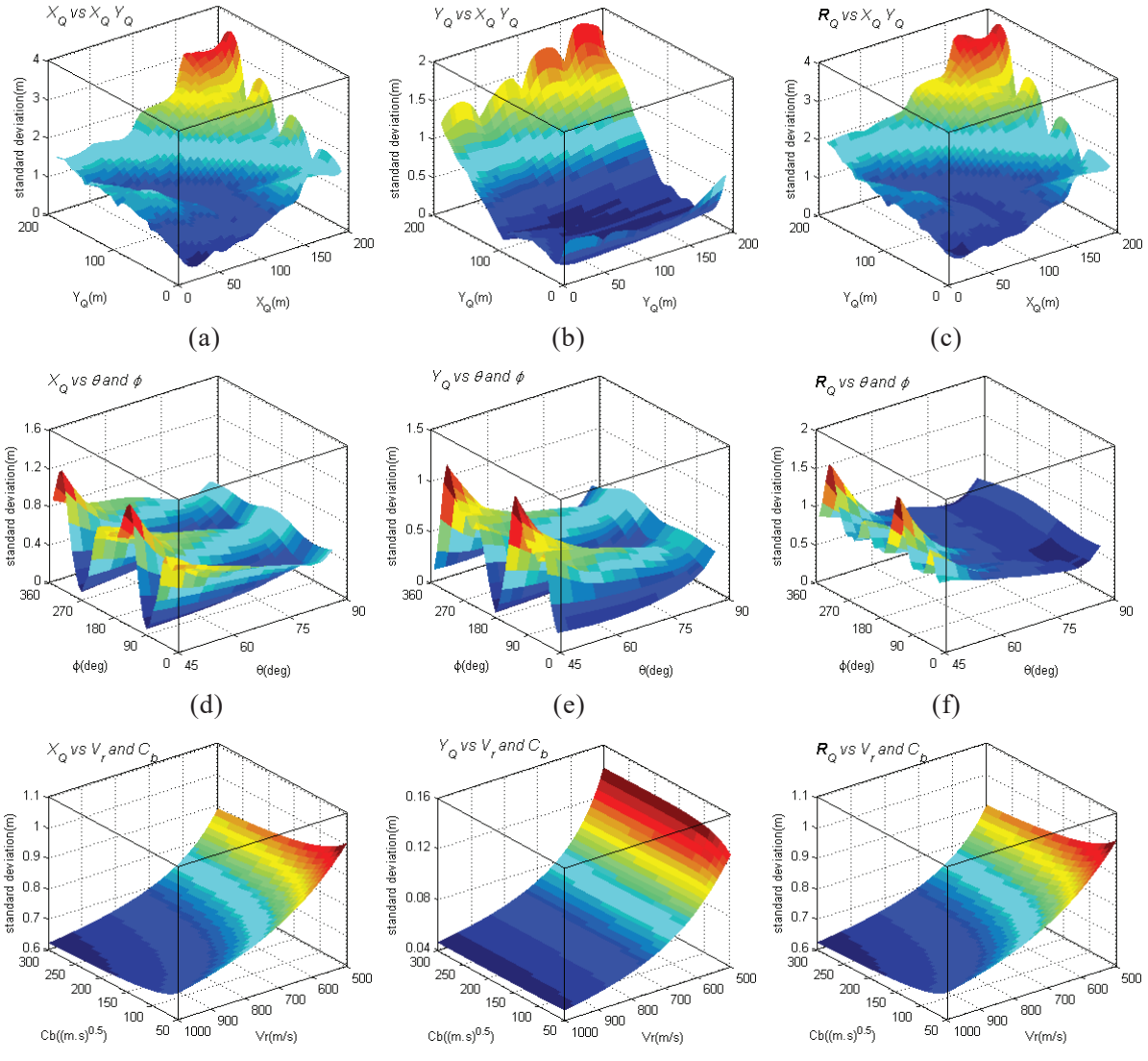

Figure 4 – Impact point error distribution versus hit position, angles and speed. (a) (d) (g) are

x-coordinate error distribution, (b) (e) (h) are y-coordinate error distribution and (c) (f) (i) are position error distribution. (a)-(c) are error distribution versus X_Q and Y_Q, (d)-(f) are error distribution versus θ and ϕ, (g)-(i) are error distribution versus V_r and C_b.

As is shown in the above figure (a)-(c), when the projectile hits the ground at different position, the error of impact point is different. Near to Sensor 9 (at (200,200,0)m), the error of impact point is large because that the DTOA algorithm is mainly based on time arrival difference between Sensor 1 and others. Points near Sensor 9 is relatively far from Sensor 1, forming a longer distance for shock wave to travel, so the accumulated error is larger, and the impact point error is larger. When the impact point is close to a sensor, the total error will reach the local minimum, because at this situation, the arrival time acquisition error is minimal, and its contribution to the total error is minimal. The X-coordinate error of impact point is larger than the Y-coordinate error in general, because the projection of the ballistic trajectory is parallel to the X-axis, and the spatial resolution of the X-axis direction decreases(14) (Imaginne in extreme cases that θ=0 and ϕ=0, and the x-coordinate estimation error increases indefinitely).

Figure 4 (d-f) shows the error distribution versus elevation angle θ and azimuth angle ϕ, it can be seen that in general, the more the trajectory is prependicular to the ground, the less impact point error is.

Figure 4 (g-i) are the error distribution versus ballistic const C_b and projectile hitting speed V_r. As the speed gets slower, the shock wave angle become greater, so the positioning error become greater.

4.4 Impact point positioning error versus sensor spacing

This is Scenaric 3, and the basic setting is the same as Scenario 1. Change the sensor spacing a and the impact point coordinate (1.6a, 1.8a, 0), the relationship between the error of impact point and different error sources is obtained. The result is shown in Figure 5.

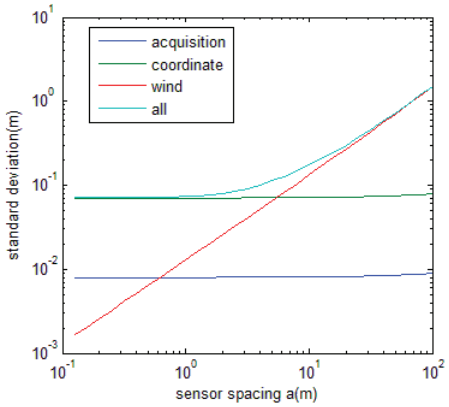

Figure 5 – Impact point error versus target scale for different error sources

Figure 5 shows that when the target size (or the sensor spacing) is greater than a certain threshold (here the threshold a=0.63, target size 2.5*2.5m), the influence of wind speed on the total error become the greatest, and linearly increases with the increase of target size. When the target surface amplitude is small, the sensor position error and the time acquisition error take the lead successively. At this time, the sensor position is usually measured by rulers, with high accuracy, so the time acquisition error has dominant influence. This conclusion is in according to the common set up in early articles.

5. CONCLUSIONS

In this paper, NLS algorithm is applied to realize the localization of the impact point of supersonic flight projectile, and the CRLB method for the positioning error estimation is improved, so that it is still applicable under the influence of the wind within level 3. Simulation results show that the improved CRLB method can truly reflect the distribution law of simulation data and can be used as a basis for analyzing the error distribution characteristics of impact points under different circumstances. According to the improved method, analysis is conducted on which error sources are dominant under different target scales, and the conclusion has certain guiding significance for the confirmation and evaluation of field array scheme.

REFERENCES

1. Rathakrishnan E. Applied gas dynamics. 2nd ed. Chichester, West Sussex, UK: John Wiley & Sons; 2019.
2. Anderson JD. Hypersonic and high-temperature gas dynamics. Reston, Virginia, USA: American Institute of Aeronautics and Astronautics; 2006.
3. Cannella M, Cappa P, Sciuto SA. A novel approach for determining the trajectory and speed of a supersonic object. Measurement Science & Technology. 2003;14(8):1485.
4. Mäkinen T, Pertilä P. Shooter localization and bullet trajectory, caliber, and speed estimation based on detected firing sounds. Applied Acoustics. 2010;71(10):902-13.
5. Levanon N. Acoustic hit indicator. IEEE Transactions on Aerospace & Electronic Systems. 2001;37(1):304-9.
6. Weinacht P, Cooper GR, Newill JF. Analytical prediction of trajectories for high-velocity direct-fire munitions. Aberdeen Proving Ground, MD: U.S. Army Research Laboratory; 2005.
7. Lo KW. Curvilinear trajectory estimation of a supersonic bullet using ballistic shock wave arrivals at asynchronous acoustic sensor nodes. Journal of the Acoustical Society of America. 2017;141(6):4543.
8. Lindgren D, Wilsson O, Gustafsson F, Habberstad H, editors. Shooter localization in wireless sensor networks. International Conference on Information Fusion; 2009.
9. Lo KW, editor Supersonic bullet trajectory estimation using ballistic shock wave arrivals at an acoustic sensor array. Proceedings of ACOUSTICS 2016; 2016 9-11 November 2016; Brisbane, Australia.
10. Völgyesi P, Balogh G, Nádas A, Nash CB, Lédeczi Á, editors. Shooter localization and weapon classification with soldier-wearable networked sensors. International Conference on Mobile Systems; 2007.
11. Lo KW, Ferguson BG. Localization of small arms fire using acoustic measurements of muzzle blast and/or ballistic shock wave arrivals. Journal of the Acoustical Society of America. 2012;132(5):2997-3017.
12. Lindgren D, Wilsson O, Gustafsson F, Habberstad H. Shooter Localization in Wireless Microphone Networks. Eurasip Journal on Advances in Signal Processing. 2010;2010(1):1-11.
13. Sengupta SK. Fundamentals of Statistical Signal Processing: Estimation Theory1993.
14. Grasing D, Ellwood B. Development of acoustic sniper localization methods and models. Proc Spie. 2010;7693:769312--13.